Computer Methods and Programs in Biomedicine

EVISE

CMPB_2019_359 | Full Length Article

Novel Atlas of Fiber Directions From Ex-Vivo DT Images of Porcine Hearts

Mia Mojica | University of Ontario Institute of Technology, Canada.

Status: **Under Review (9 days)** | Submitted: **17/Mar/2019**

Zip File

Overview

Other Authors Show Details

Mihaela Pop (Sunnybrook Research Institute), Maxime Sermesant (INRIA Sophia Antipolis), Mehran Ebrahimi (University of Ontario Institute of Technology)

Abstract

Background and Objective Cardiac MR image-based predictive models integrating statistical atlases of heart anatomy and fiber orientations can aid in better diagnosis of cardiovascular disease, a major cause of death worldwide. Such atlases have been built from diffusion tensor (DT) images and can be used in anisotropic models for personalized computational electro-mechanical simulations when the fiber directions from DTI are not available. Here, we propose a framework for constructing a statistical fiber atlas from high resolution ex-vivo DT images of porcine hearts. Methods High-resolution diffusion tensor images were acquired to determine the voxel-wise preferential direction of diffusion. A mean cardiac volume was then generated through an iterative groupwise scheme. The final set of transformations from the averaging process were then used to project the original DT fields to the same coordinate system as that of the mean and the final registered volumes, thereby allowing the computation of an average DT field and the associated fiber architecture. Results Multilevel elastic registration was able to effectively match the hearts to the reference geometries, as demonstrated by the increase in the Jaccard indices post-registration. This allowed the groupwise framework to converge to a reasonable average geometry after a few iterations. Local orientations of diffusion were preserved through the Finite Strain reorientation method implemented. Finally, the leave-one-out cross-validation only resulted to small errors for the mean FA and fiber length. Conclusions We successfully created the first cardiac fiber atlas for porcine hearts. In addition, we proposed a simple pipeline for building a statistical cardiac atlas computed from a small database. A morphological average cardiac geometry was computed via a computationally efficient algorithm without the need for selecting landmarks. Meanwhile, the associated average fiber architecture was built from reoriented DT fields that preserved the local fiber directions. Tensor statistics extracted from the leave-one-out validation of the fiber atlas indicate that constructing a statistical fiber atlas even from a small database of pig hearts could accurately describe the fiber architecture of a healthy pig heart.

Keywords

cardiac atlas; MRI; diffusion tensor imaging; elastic registration; tensor transformation

Additional Information View

References View

Novel Atlas of Fiber Directions Built From *Ex-Vivo* Diffusion Tensor Images of Porcine Hearts

Mia Mojica, Mehran Ebrahimi

Faculty of Science, University of Ontario Institute of Technology, ON, Canada

Maxime Sermesant

Asclepios Team, INRIA Sophia Antipolis, France

Mihaela Pop

Department of Medical Biophysics, University of Toronto, Sunnybrook Research Institute, ON, Canada

Abstract

Background and Objective

Cardiac MR image-based predictive models integrating statistical atlases of heart anatomy and fiber orientations can aid in better diagnosis of cardiovascular disease, a major cause of death worldwide. Such atlases have been built from diffusion tensor (DT) images and can be used in anisotropic models for personalized computational electro-mechanical simulations when the fiber directions from DTI are not available. Here, we propose a framework for constructing a statistical fiber atlas from high resolution *ex-vivo* DT images of porcine hearts.

Methods

High-resolution diffusion tensor images were acquired to determine the voxel-wise preferential direction of diffusion. A mean cardiac volume was then generated through an iterative groupwise scheme. The final set of transformations from the averaging process were then used to project the original DT fields to

Email addresses: mia.mojica@uoit.ca (Mia Mojica), mehran.ebrahimi@uoit.ca (Mehran Ebrahimi), maxime.sermesant@inria.fr (Maxime Sermesant), mihaela.pop@utoronto.ca (Mihaela Pop)

the same coordinate system as that of the mean and the final registered volumes, thereby allowing the computation of an average DT field and the associated fiber architecture.

Results

Multilevel elastic registration was able to effectively match the hearts to the reference geometries, as demonstrated by the increase in the Jaccard indices post-registration. This allowed the groupwise framework to converge to a reasonable average geometry after a few iterations. Local orientations of diffusion were preserved through the Finite Strain reorientation method implemented. Finally, the leave-one-out cross-validation only resulted to small errors for the mean FA and fiber length.

Conclusions

We successfully created the first cardiac fiber atlas for porcine hearts. In addition, we proposed a simple pipeline for building a statistical cardiac atlas computed from a small database. A morphological average cardiac geometry was computed via a computationally efficient algorithm without the need for selecting landmarks. Meanwhile, the associated average fiber architecture was built from reoriented DT fields that preserved the local fiber directions. Tensor statistics extracted from a leave-one-out validation of the fiber atlas indicate that constructing a statistical fiber atlas even from a small database of pig hearts could accurately describe the fiber architecture of a healthy pig heart.

Keywords: cardiac atlas, MRI, diffusion tensor imaging, elastic registration, tensor transformation

---

1. Introduction

The structural remodeling of the myocardial fibers is a main determinant of cardiac function as electrical propagation within the heart is highly anisotropic

and occurs fastest in the long axis of the fibers [1, 2, 3]. For instance, discontinuities in the laminar arrangement of cardiac myocytes could trigger a nonuniform and potentially asymmetric spread of electrical activation in the ventricles and could ultimately lead to cardiac arrhythmia [4]. Thus, developing more insights on the connections between fibers and the underlying physiological structure of the heart could help in the diagnosis and treatment-planning in cardiovascular diseases (CVD).

Until recently, myocardial fiber directions have only been mapped out through histological slices [2, 5, 6, 7]. Diffusion tensor MR imaging now provides an alternative and less invasive way to characterize fiber orientations in healthy state, which can in turn be integrated into predictive image-based heart models [8, 9] and statistical atlases [10, 11].

Statistical atlases of cardiac anatomy have been built from diffusion tensor (DT) images of human, canine, and rat hearts [12, 7, 13]. Of particular interest in this paper is constructing one from pig hearts, which could provide a good alternative to human and canine hearts as the cardiac anatomies of the three species are very similar [14].

In [7], they presented a detailed computational framework to build a statistical fiber atlas from 9 *ex-vivo* canine hearts. Their framework started with a groupwise registration of the anatomical MR images of the subjects, followed by a transformation of associated diffusion tensor (DT) fields. They then proceeded to compute the mean DT fields and measured the variability of eigenvalues and eigenvectors, which indicate the magnitude and preferential direction of diffusion. They also computed diffusion tensor statistics characterizing cardiac fiber and laminar sheet orientations. Most importantly, they found good inter-species stability of fiber orientations between the canine and human atlas.

Lombaert et al. [12] built the first atlas of the human heart from *ex-vivo* DT-MRI acquisitions of 10 healthy hearts. Their pipeline involved segmentation of myocardium and blood mass on each subject, construction of a morphological atlas through an iterative reference update process coupled with Symmetric Diffeomorphic Log-Demons on the unweighted images and myocardium masks,

and deformation of tensor fields to the morphological atlas. They found that the fiber orientation dispersion across the population concurred with results from previous studies on mammals. Another atlas of the human heart, this time from *in-vivo* acquisitions, was built by Toussaint *et al.* [10], where they used sparse 2D DTI slices and the Prolate Spheroidal model of the heart to create a 3D reconstruction of the fiber architecture in the left ventricle.

In [13], rat and dog myocardial atlases (also obtained through Log Demons) were used to estimate the Generalized Helicoid Model [15, 16] and to characterize the properties of the local arrangement of myofibers via three biologically meaningful curvature parameters. They concluded that the turning of fibers within a transmural penetration from epicardium to endocardium is an important descriptor of fiber bundle variability.

Nowadays, most translational cardiovascular experiments and associated simulation-based predictive modeling are carried out using porcine models of normal and diseased hearts [17, 18, 9]. Porcine heart models mimic very well normal human heart anatomy, physiology and pathology, which motivates us to develop a high resolution DTI-based porcine fiber atlas that could be beneficial for various preclinical studies (i.e., from disease assessment to electro-mechanical simulations).

In this paper, we present a simple pipeline employing anatomical and fiber information from DTI to map out fiber directions in healthy pig hearts. To accomplish this, we build both a morphological and a fiber atlas through a combination of groupwise registration and diffusion tensor transformation techniques that are both computationally efficient and effective in keeping the diffusion information from each subject. The groupwise framework is coupled with a pairwise registration algorithm that uses only intensity information to match the subjects to the reference volumes, thereby eliminating the need for landmarks and speeding up the computation of a representative cardiac volume. It also provides the displacement fields necessary to fuse information from different diffusion tensor fields and allows for analysis of diffusion properties within the population.

2. Methods

A diagram of our workflow is shown in Figure 1. High-resolution diffusion tensor images were acquired to determine the voxel-wise preferential direction of diffusion. A mean cardiac volume was then generated through an iterative groupwise scheme. The final set of transformations from the averaging process were then used to project the original DT fields to the same coordinate system as that of the mean and the final registered volumes, thereby allowing the computation of an average DT field and the associated fiber architecture.

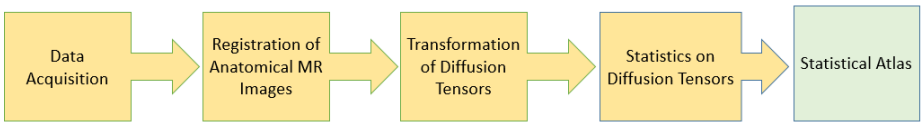

Figure 1: Key steps to building a statistical cardiac fiber atlas. DT-MR images were acquired, and then an groupwise registration was performed to normalize the anatomical structures of the 8 subjects. The transformations registering the subjects to the mean geometry were used to reorient the tensors associated to each heart, thereby allowing the computation of the average DT field.

2.1. Data

Diffusion-weighted images (DWI) are generated by exciting water molecules using different magnetic field gradients, which allow the estimation of a diffusion tensor that characterizes the type, magnitude, and direction of diffusion at every voxel [19, 20]. It is a symmetric positive definite matrix

$$D = \begin{bmatrix} d_{xx} & d_{xy} & d_{xz} \\ d_{xy} & d_{yy} & d_{yz} \\ d_{xz} & d_{yz} & d_{zz} \end{bmatrix} \tag{1}$$

whose entries along the main diagonal are diffusion coefficients measured along the principal (x-, y-, and z-) axes. Meanwhile, the off-diagonal entries describe the Brownian motion between each pair of principal directions.

At least six DWIs and an unweighted baseline image are generated to calculate the entries of a diffusion tensor. For each DWI, the MR signal S is

influenced by the proton density P, repetition and echo times TR and TE, signal decay times after excitation T_1 and T_2, the diffusion-weighting factor b, and the diffusion coefficient d. It is given by

$$S = P\left(1 - e^{-TR/T_1}\right) e^{-TE/T_2} e^{-bd}. \tag{2}$$

In Equation (2), the diffusion coefficient d represents the Brownian motion of water molecules. It is obtained by comparing a weighted signal S_1 against an unweighted signal S_0 while keeping all the parameters fixed, except for the diffusion-weighting factors $b_0 = 0$ and $b_1 > 0$ of the two experiments, i.e.,

$$d = -\ln\left(\frac{S_1}{S_0}\right) / \left(b_1 - b_0\right).$$

The value of d is calculated for each gradient direction applied to the MR image and subsequently expressed as linear combination of the d_{ij}'s in Equation (1). This results to a system of equations whose solution gives the entries of the diffusion tensor.

In our experiments, all high resolution DT MR images were acquired on a 1.5T GE Signa Excite scanner in explanted healthy pig hearts ($N = 8$) at sub-millimetric resolution by using the MR parameters TE = 35 ms, TR = 700 ms, echo train length = 2, b-value = 0 for the unweighted MR images and b = 500-600 s/mm^2 for the seven diffusion gradients, respectively [21]. Notably, the total MR imaging time was approximately 10 hours per heart, which is not feasible for *in-vivo* patient studies.

2.2. Pairwise Elastic Registration

Mathematically, the task of finding the optimal transformation y from a subject $\mathcal{T} : \Omega \subset \mathbb{R}^n \to \mathbb{R}$ to a reference $\mathcal{R} : \Omega \subset \mathbb{R}^n \to \mathbb{R}$ is given by the following minimization problem:

$$\min_y \mathcal{J}[y] = \mathcal{D}[\mathcal{T}[y], \mathcal{R}] + \mathcal{S}[y], \tag{3}$$

where $y : \Omega \to \mathbb{R}^n$ and $\mathcal{T}[y]$ is a transformed version of the subject.

The above function consists of two parts. The distance measure $\mathcal{D}$ and the regularization term $\mathcal{S}$. The former quantifies the similarity between the transformed version of the subject and the reference, while the latter serves to add constraints to the solution space.

The distance measure used in our experiments was the Sum of Squared Differences (SSD) given by

$$\mathcal{D}\left[\mathcal{T}\left[y\right], \mathcal{R}\right] = \frac{1}{2}\int_{\Omega} \left(\mathcal{T}[y](x) - \mathcal{R}(x)\right)^2 \, dx. \tag{4}$$

The regularization term $\mathcal{S}[y]$ enforces the functional to lead to a unique minimizer. In our experiments, we used the elastic potential of the transformation y for our regularization term. It is given by

$$\mathcal{S}[y] = \frac{1}{2}\int_{\Omega} \mu \left\langle \nabla y, \nabla y \right\rangle + (\lambda + \mu)(\nabla \cdot y)^2 dx,$$

where λ and μ are the Lamé constants [22]. The elastic regularizer is the elastic potential measuring the energy introduced by deforming an elastic material [23].

2.3. Groupwise Registration

Groupwise registration was used to normalize the cardiac measurements and obtain an average cardiac volume. Every iteration in the groupwise algorithm was initialized by the collection of pairwise transformations registering each heart to the current reference geometry.

The reference geometries were updated as

$$\mathcal{R}^{n+1}_{\text{mean}}(\mathrm{x}) = \frac{1}{N}\sum_{i=1}^{N} \mathcal{T}_i \left(y_i^n \circ \left[y^n_{\text{mean}}\right]^{-1}(\mathrm{x})\right), \tag{5}$$

where

- x denotes the original grid,
- N refers to the number of heart volumes $\mathcal{T}_i$ in the dataset,
- y_i^n registers the i^{th} heart to the n^{th} reference, and

- the mean of the transformations registering the hearts to the current reference is denoted by

$$y^n_{\text{mean}} = \frac{1}{N}\sum_{i=1}^{N} y^n_i.$$

2.4. Tensor Reorientation and Average Diffusion Tensor Field

The registration step modified the original frames of reference of the subjects and projected them onto the same coordinate system. Naturally, the diffusion tensors linked to these registered subjects had to be reoriented according to these modifications to allow for subject-to-subject comparisons and, more importantly, the computation of an average DT field.

Using the Finite Strain method, each diffusion tensor D_i was transformed using the rotation component of the associated local deformation gradient $A = RU$ obtained via polar decomposition. The transformed tensor D'_i is given by

$$D'_i = R \cdot D_i \cdot R^T.$$

Diffusion tensors are positive-definite matrices. Therefore, they do not form a vector space and standard linear statistical techniques do not apply [24]. Log-Euclidean metrics have been demonstrated to circumvent the absence of vector space structure and incompatibility of the classical Euclidean framework on tensors while preserving their positive-definiteness [25].

The mean $\overline{D}_{\log}$ of the reoriented tensors D'_i for every voxel X is given by

$$\overline{D}_{\log}(X) = \exp\left(\frac{1}{N}\sum_{i=1}^{N} \log\left(D'_i\left(X\right)\right)\right). \tag{6}$$

3. Experiments and Results

Multilevel elastic registration was performed to align the hearts to the current reference volume. At every level, the optimization problem was solved via Gauss-Newton (GN) method coupled with an Armijo line search.

Shown in Figure 2 are some results obtained after implementing the pairwise registration method discussed in the previous section. In addition, we also calculated the Jaccard similarity coefficients to quantify the similarity between two

cardiac volumes. Given a subject $\mathcal{T}$ and a reference $\mathcal{R}$, the Jaccard similarity coefficient pre- and post-registration are defined as

$$J\left[\mathcal{T},\mathcal{R}\right]=\frac{\left|\mathcal{T}\cap\mathcal{R}\right|}{\left|\mathcal{T}\cup\mathcal{R}\right|}\quad\text{and}\quad J\left[\mathcal{T}\left[y\right],\mathcal{R}\right]=\frac{\left|\mathcal{T}\left[y\right]\cap\mathcal{R}\right|}{\left|\mathcal{T}\left[y\right]\cup\mathcal{R}\right|},$$

respectively. The computed similarity indices are shown in Figure 1.

Meanwhile, groupwise registration was implemented to generate a sequence of updates to the reference volume. In our experiments, an arbitrarily chosen heart in the dataset served as the initial reference, and the reference volumes converged to the average geometry shown in Figure 3(a). The algorithm was terminated when the average change in intensity values for the iteration was below 5% of the initial value. This error evolution of the groupwise algorithm is shown in Figure 5(b).

All the transformations aligning the hearts to the final reference were then used to reorient the tensors and project them onto a common frame of reference. Illustrated in Figure 4 are the original and transformed tensors of one of the subjects. The following color-coding indicates the orientation of the tensors: red=left-right, green=anterior-posterior, and blue=superior-inferior. The average DT field was computed using Equation (6) following the tensor transformations, and the associated average fiber architecture was visualized using MedInria [26].

Finally, we performed a leave-one-out validation. The same pipeline was implemented after excluding an arbitrarily chosen heart in the dataset. The average DT field and fiber architecture obtained from 7 hearts is shown in Figure 5(a). In Figure 5(b), we plotted the convergence of the groupwise algorithm for both experiments by measuring the mean change in signal intensities between successive reference cardiac volumes. We also tracked the change in the mean fractional anisotropy (FA) and fiber lengths in the mean geometries. Fractional anisotropy is a scalar FA ($0\leq FA\leq 1$) that quantifies the degree or type of diffusion. It can be computed from the eigenvalues of the diffusion tensor D as

follows:

$$FA = \sqrt{\frac{(\lambda_1 - \lambda_2)^2 + (\lambda_2 - \lambda_3)^2 + (\lambda_3 - \lambda_1)^2}{2(\lambda_1^2 + \lambda_2^2 + \lambda_3^2)}},$$

where λ_1, λ_2, and λ_3 are the eigenvalues arranged in order of decreasing magnitude. Diffusion is isotropic if $\lambda_1 \approx \lambda_2 \approx \lambda_3$ and FA is close to zero. On the other hand, diffusion is anisotropic if there is a dominant eigenvalue $\lambda_1 >> \lambda_2 > \lambda_3$, resulting to an FA-value that is closer to 1. The mean FA for the atlas constructed from 8 and 7 hearts, respectively, was 0.192861 and 0.191071. The mean fiber lengths from the two experiments were 88.208 mm and 90.6473 mm. More details can be found in Figure 5(c).

Pairwise and groupwise registration were implemented in MATLAB on a machine running on Intel(R) Core(TM) i5-8250U CPU @ 1.80GHz with 16GB of RAM. All tensors were reoriented and averaged using a workstation with Intel(R) Xeon(R) CPU E5-1620 v2 @ 3.70GHz and 16GB of RAM.

4. Discussion

Multilevel elastic registration was able to effectively match the hearts to the reference geometries. As demonstrated by the Jaccard indices in Figure 2(b), all the hearts generally started with relatively low similarities to the reference geometries. The pairwise method we employed bumped the Jaccard indices up to as much as 97.68%, which corresponds to a 208.60% increase in similarity.

The groupwise framework converged to a reasonable average geometry after just eight iterations. The average change in intensity values between consecutive reference geometries dropped from approximately 0.040 to 0.001, where the range of intensities in the anatomical MR images was $[0, 1]$.

Next, we observe the action of the Finite Strain method on the tensors. An important aspect of tensor reorientation is that it should preserve the local orientation of diffusion. As illustrated in Figure 4, the counterclockwise rotation of tensors from the left ventricle (LV) to the endocardium on the septum and from the epicardium to the endocardium on the LV free wall was retained after reorienting the tensors using Finite Strain. This implies that the method is

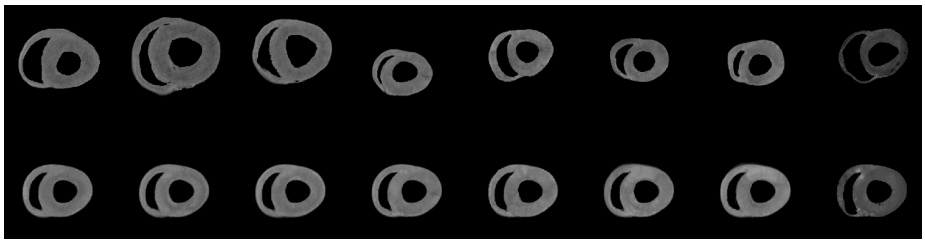

(a) Raw and registered versions of the hearts in the dataset

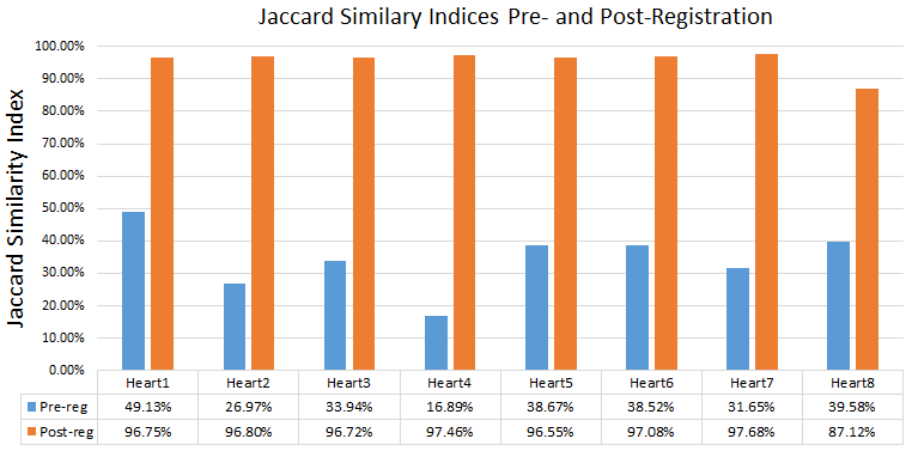

	Heart1	Heart2	Heart3	Heart4	Heart5	Heart6	Heart7	Heart8
Pre-reg	49.13%	26.97%	33.94%	16.89%	38.67%	38.52%	31.65%	39.58%
Post-reg	96.75%	96.80%	96.72%	97.46%	96.55%	97.08%	97.68%	87.12%

(b) Jaccard similarity coefficients

Figure 2: Pairwise 3D to 3D registration. (a) First Row: Center slices (short axis) of the unregistered hearts, Second Row: Registered/Transformed versions of the hearts, (b) Jaccard indices quantifying the similarity between the subjects and the final reference volume before and after registration.

suited for registration of DT-MR images [7]. It follows that the computed final average DT field and its corresponding fiber architecture picked up the directional information on diffusion from all the subjects.

We remark that the leave-one-out cross-validation only resulted to small errors of 0.93% and 2.77% for the mean FA and fiber length. This implies that constructing a statistical fiber atlas even from a small database of pig hearts could accurately describe the fiber architecture of a healthy pig heart.

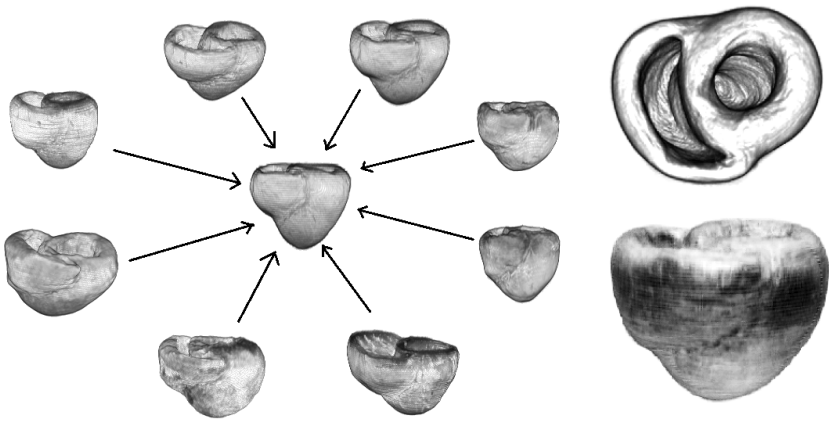

(a) **(b)**

Figure 3: Groupwise registration and average geometry. (a) The dataset and the implementation diagram for one iteration of the groupwise registration scheme and (b) superior and anterior views of the average geometry obtained from 8 porcine hearts.

5. Conclusions

We successfully created the first cardiac fiber atlas for porcine hearts. In addition, we proposed a simple pipeline for building a statistical cardiac atlas. An average cardiac geometry was computed from a small database via a computationally efficient algorithm without the need for selecting landmarks. We also reoriented the diffusion tensors of each heart while preserving their local fiber directions and subsequently obtained the average diffusion tensor field and cardiac fiber architecture. Future work will focus on obtaining more tensor statistics to better understand the underlying fiber and laminar sheet structure, performing intra- and inter-species comparisons to check for correspondence of fiber and laminar sheet orientations, and using the fiber atlas for electro-mechanical simulations to predict cardiac function.

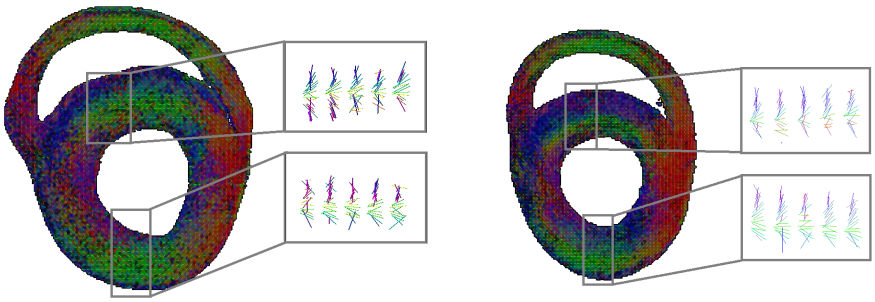

(a) **(b)**

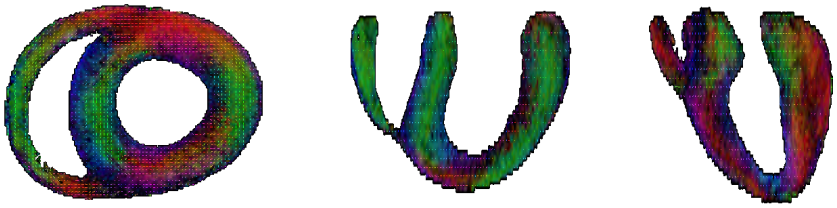

(c)

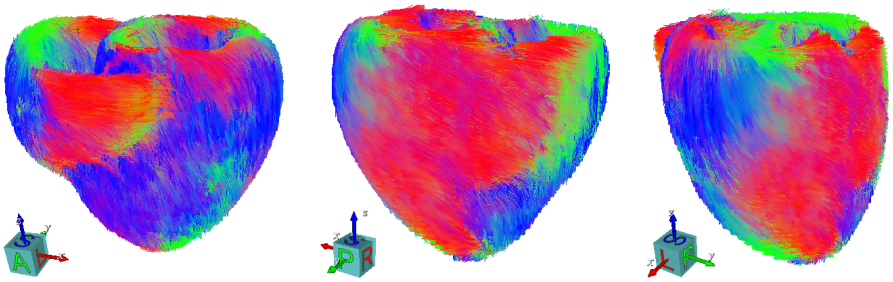

(d)

Figure 4: Preservation of tensor orientations, and tensor and fiber atlas. (a) The original and (b) transformed DT field of one of the subjects. Zoomed in sections show the tensors viewed transmurally from an area in the septum and the LV free wall. Observe that the geometric features and the counter-clockwise rotation of the diffusion tensor fields were preserved. (c) the average DT field and the associated (d) average fiber architecture obtained from the 8 porcine hearts.

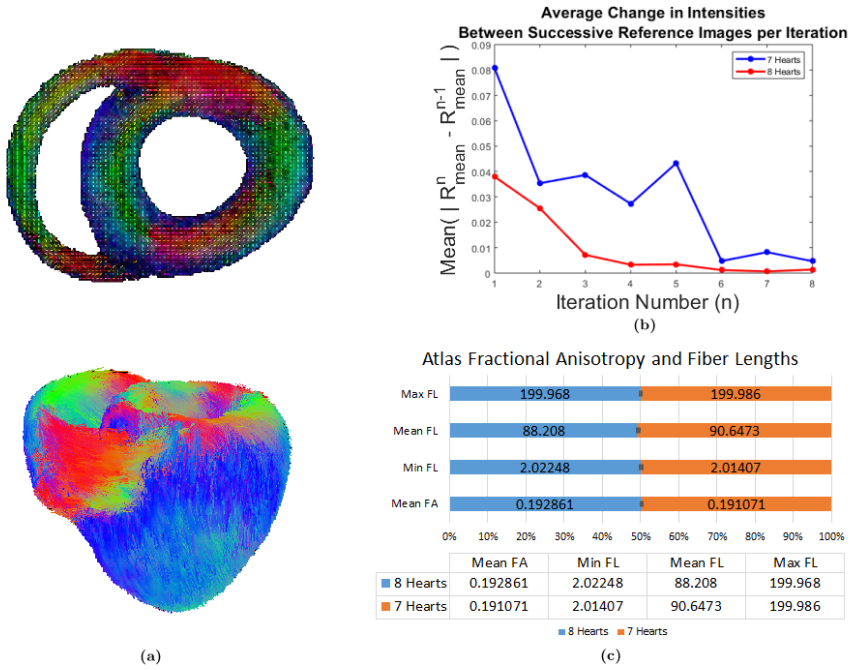

Figure 5: Leave-One-Out validation. (a) Average DT field and fiber architecture computed from 7 hearts, (b) error evolution of the groupwise scheme for the two experiments given by average change in intensity between two consecutive reference cardiac volumes, and (c) a stacked bar chart and table of values showing the mean FA, statistics on fiber lengths (in mm), and error bars from the constructed atlases.

6. Acknowledgments

This work was supported in part by an NSERC Discovery grant and Deborah Saucier Early Researcher Award for Dr. Mehran Ebrahimi, and an Inria - Associated team grant for Drs. Mihaela Pop and Maxime Sermesant. Mia Mojica is supported by an Ontario Trillium Scholarship (OTS).

References

[1] M. Burger, S. Kälz, Anisotropic conduction in electrocardiology.

[2] D. F. Scollan, A. Holmes, R. Winslow, J. Forder, Histological validation of myocardial microstructure obtained from diffusion tensor magnetic resonance imaging, American Journal of Physiology-Heart and Circulatory Physiology 275 (6) (1998) H2308–H2318.

[3] P. Helm, M. F. Beg, M. I. Miller, R. L. Winslow, Measuring and mapping cardiac fiber and laminar architecture using diffusion tensor MR imaging, Annals of the New York Academy of Sciences 1047 (1) (2005) 296–307.

[4] D. A. Hooks, K. A. Tomlinson, S. G. Marsden, I. J. LeGrice, B. H. Smaill, A. J. Pullan, P. J. Hunter, Cardiac microstructure: implications for electrical propagation and defibrillation in the heart, Circulation research 91 (4) (2002) 331–338.

[5] E. Hsu, A. Muzikant, S. Matulevicius, R. Penland, C. Henriquez, Magnetic resonance myocardial fiber-orientation mapping with direct histological correlation, American Journal of Physiology-Heart and Circulatory Physiology 274 (5) (1998) H1627–H1634.

[6] P. Nielsen, I. Le Grice, B. Smaill, P. Hunter, Mathematical model of geometry and fibrous structure of the heart, American Journal of Physiology-Heart and Circulatory Physiology 260 (4) (1991) H1365–H1378.

[7] J.-M. Peyrat, M. Sermesant, X. Pennec, H. Delingette, C. Xu, E. R. McVeigh, N. Ayache, A computational framework for the statistical analysis of cardiac diffusion tensors: application to a small database of canine hearts, IEEE transactions on medical imaging 26 (11) (2007) 1500–1514.

[8] M. Pop, M. Sermesant, D. Lepiller, M. V. Truong, E. R. McVeigh, E. Crystal, A. Dick, H. Delingette, N. Ayache, G. A. Wright, Fusion of optical imaging and MRI for the evaluation and adjustment of macroscopic models of cardiac electrophysiology: a feasibility study, Medical image analysis 13 (2) (2009) 370–380.

[9] M. Pop, M. Sermesant, T. Mansi, E. Crystal, S. Ghate, J.-M. Peyrat, I. Lashevsky, B. Qiang, E. McVeigh, N. Ayache, et al., Correspondence between simple 3-d MRI-based computer models and in-vivo ep measurements in swine with chronic infarctions, IEEE Transactions on Biomedical Engineering 58 (12) (2011) 3483.

[10] N. Toussaint, M. Sermesant, C. T. Stoeck, S. Kozerke, P. G. Batchelor, In vivo human 3d cardiac fibre architecture: reconstruction using curvilinear interpolation of diffusion tensor images, in: International Conference on Medical Image Computing and Computer-Assisted Intervention, Springer, 2010, pp. 418–425.

[11] N. Toussaint, C. T. Stoeck, T. Schaeffter, S. Kozerke, M. Sermesant, P. G. Batchelor, In vivo human cardiac fibre architecture estimation using shape-based diffusion tensor processing, Medical image analysis 17 (8) (2013) 1243–1255.

[12] H. Lombaert, J.-M. Peyrat, P. Croisille, S. Rapacchi, L. Fanton, F. Cheriet, P. Clarysse, I. Magnin, H. Delingette, N. Ayache, Human atlas of the cardiac fiber architecture: study on a healthy population, IEEE transactions on medical imaging 31 (7) (2012) 1436–1447.

[13] E. Piuze, H. Lombaert, J. Sporring, G. J. Strijkers, A. J. Bakermans, K. Siddiqi, Atlases of cardiac fiber differential geometry, in: International

Conference on Functional Imaging and Modeling of the Heart, Springer, 2013, pp. 442–449.

[14] M. Mojica, M. Pop, M. Sermesant, M. Ebrahimi, Multilevel non-parametric groupwise registration in cardiac MRI: Application to explanted porcine hearts, in: International Workshop on Statistical Atlases and Computational Models of the Heart, Springer, 2017, pp. 60–69.

[15] E. Piuze, P. G. Kry, K. Siddiqi, Generalized helicoids for modeling hair geometry, in: Computer Graphics Forum, Vol. 30, Wiley Online Library, 2011, pp. 247–256.

[16] E. Piuze, J. Sporring, K. Siddiqi, Moving frames for heart fiber geometry, in: International Conference on Information Processing in Medical Imaging, Springer, 2013, pp. 524–535.

[17] Y. Suzuki, A. C. Yeung, F. Ikeno, The representative porcine model for human cardiovascular disease, BioMed Research International 2011.

[18] M. Pop, M. Sermesant, G. Liu, J. Relan, T. Mansi, A. Soong, J.-M. Peyrat, M. V. Truong, P. Fefer, E. R. McVeigh, et al., Construction of 3d mr image-based computer models of pathologic hearts, augmented with histology and optical fluorescence imaging to characterize action potential propagation, Medical image analysis 16 (2) (2012) 505–523.

[19] L. J. O'Donnell, C.-F. Westin, An introduction to diffusion tensor image analysis, Neurosurgery Clinics 22 (2) (2011) 185–196.

[20] S. Mori, J. Zhang, Principles of diffusion tensor imaging and its applications to basic neuroscience research, Neuron 51 (5) (2006) 527–539.

[21] M. Pop, N. R. Ghugre, V. Ramanan, L. Morikawa, G. Stanisz, A. J. Dick, G. A. Wright, Quantification of fibrosis in infarcted swine hearts by ex vivo late gadolinium-enhancement and diffusion-weighted MRI methods, Physics in medicine and biology 58 (15) (2013) 5009.

[22] M. E. Gurtin, An introduction to continuum mechanics, Vol. 158, Academic press, 1982.

[23] J. Modersitzki, FAIR: Flexible algorithms for image registration, Vol. 6, SIAM, 2009.

[24] P. T. Fletcher, S. Joshi, Principal geodesic analysis on symmetric spaces: Statistics of diffusion tensors, in: Computer Vision and Mathematical Methods in Medical and Biomedical Image Analysis, Springer, 2004, pp. 87–98.

[25] V. Arsigny, P. Fillard, X. Pennec, N. Ayache, Log-euclidean metrics for fast and simple calculus on diffusion tensors, Magnetic Resonance in Medicine: An Official Journal of the International Society for Magnetic Resonance in Medicine 56 (2) (2006) 411–421.

[26] N. Toussaint, J.-C. Souplet, P. Fillard, et al., Medinria: Medical image navigation and research tool by INRIA, in: Proc. of MICCAI, Vol. 7, 2007, p. 280.